STRUCTURAL CONTROL AND HEALTH MONITORING
Struct. Control Health Monit. 2014; **21**:962–978
Published online 6 November 2013 in Wiley Online Library (wileyonlinelibrary.com). DOI: 10.1002/stc.1624

Blind denoising of structural vibration responses with outliers via principal component pursuit

Yongchao Yang[1] and Satish Nagarajaiah[1,2,*,†]

[1]*Department of Civil and Environmental Engineering, Rice University, Houston, TX 77005, U.S.A.*
[2]*Department of Mechanical Engineering and Material Science, Rice University, Houston, TX 77005, U.S.A.*

SUMMARY

Structural vibration responses themselves contain rich dynamic information, exploiting which can lead to tackling the challenging problem: simultaneous denoising of both gross errors (outliers) and dense noise that are not uncommon in the data acquisition of SHM systems. This paper explicitly takes advantage of the fact that typically only few modes are active in the vibration responses; as such, it is proposed to re-stack the response data matrix to guarantee a low-rank representation, through which even heavy gross and dense noises can be efficiently removed via a new technique termed principal component pursuit (PCP), without the assumption that sensor numbers exceed mode numbers that used to be made in traditional methods.

It is found that PCP works extremely well under broad conditions with the simple but effective strategy no more than reshaping the data matrix for a low-rank representation. The proposed PCP denoising algorithm overcomes the traditional PCA (or SVD) and low-pass filter denoising algorithms, which can only handle dense (Gaussian) noise. The application of PCP on the health monitoring data of the New Guangzhou TV Tower (Canton Tower) shows its potential for practical usage. Copyright © 2013 John Wiley & Sons, Ltd.

Received 18 July 2013; Accepted 16 September 2013

KEY WORDS: principal component pursuit; denoising; principal component analysis; low-rank representation; structural health monitoring

1. INTRODUCTION

With more understanding of the importance of the structural safety and integrity during their performance life cycle, it has recently become a common practice to embed a sensor network to continuously monitor the structural behaviors. Many of such exercises are devoted to monitoring of seismic structural responses [1–3]. For example, the California Strong Motion Instrumentation Program [4,5] has installed across California seismic monitoring sensor networks in more than 600 ground motion stations as well as 200 civil infrastructures; the collected data are extremely valuable for studying the seismic performance of structures [6–11].

More recently, the data-intensive issue has risen in the SHM community. Much of the attention stems from the excitement that comprehensive SHM systems have served as 'mandate' instrumentations for newly built large-scale civil structures. For example, many landmark suspension bridges and high-rise buildings or towers have been equipped with even dense sensors: the Tsing Ma Bridge (1997) in Hong Kong, the Canton Tower (2010) in Guangzhou, China, and the Stonecutters Bridge (2009) in Hong Kong, with more than 280, 800, and 1500 sensors [12–14], respectively. The overwhelmingly voluminous data continuously collected from the SHM system await efficient algorithms to extract useful structural information for online monitoring as well as offline long-term performance analysis.

*Correspondence to: Satish Nagarajaiah, CEVE and MEMS, Rice University, Houston, TX 77005, USA.
†E-mail: Satish.Nagarajaiah@rice.edu

Among many data mining problems associated with the seismic monitoring or SHM data, one fundamental problem would be obtaining truly reliable structural response data for further analysis; such is referred to as the data cleaning process [15]. Unfortunately, the real-world measured data typically contain considerable noise or errors that would significantly affect further analysis. For example, Figure 1 shows the ambient vibration response data of the Canton Tower recorded from the SHM system; it contains remarkable sparse outliers (gross errors), which call for efficient data cleaning or denoising algorithms before they can be used for structural assessment.

Many researchers in structural dynamics and SHM communities have studied the denoising problem by using various techniques. SVD (closely related to the PCA) was proposed for noise reduction in vibration signals of rotating machinery [17]. A Bayesian wavelet packet denoising scheme was developed for system identification; this approach can not only remove the present noise but also characterize the noise level of the data [18]. Also, an optimal global projection denoising method was proposed to better capture the nonlinear fault features in the vibration signals of the shaft orbits [19]. For removal of the noise in the acoustic emission signals in local SHM damage inspection, particle-filter-based method was also formulated and found to outperform other filtering methods [20]. Noise suppression method was also reported to facilitate robust damage identification in beam-type structures [21].

These existing methods, however, are mostly devoted to removal of (Gaussian-type) dense small noise in vibration signals; little efforts—if not none—have been made to handle the outliers (sparse spikes with arbitrarily large amplitudes unreasonably present in the signals), which are not uncommon in practical seismic monitoring or SHM systems, such as those shown in Figure 1. Such outliers may arise because of sensor imperfection, instrumentation error, sensor failure, and environmental factors or simply because some measurements are considerably inconsistent.

This paper develops a new denoising algorithm in order to simultaneously deal with both dense noise and outliers by exploiting the intrinsic dynamic information contained in the structural responses. The developed method cast the denoising problem into the framework of low-dimensional matrix recovery in the presence of both grossly corrupted errors and small dense noise. First, a simple re-stacking strategy is proposed to guarantee a low-rank representation of the structural response data matrix corrupted by noise, by taking advantage of the observation that mode information (typically few are active, hence the rank of the matrix) remains invariant regardless of the reshaping of the data matrix. The reshaped data matrix is then decomposed into a superposition of a low-rank matrix plus a sparse outlier matrix with small dense noise via a new technique termed principal component pursuit (PCP) [22,23]. The denoised low-rank data matrix is finally re-stacked back to its original shape as the estimation of the noise-free data matrix.

The established PCP method for denoising of structural responses is much inspired by the recent groundbreaking developments of sparse representations [24,25] and compressed sensing [26–28], which have seen successful applications in SHM and structural dynamics [29–32]. While sparse representations and compressed sensing exploit the sparsity property of a vector signal, PCP, as a new high-dimensional data analysis method, explicitly considers the structured sparsity inherent in

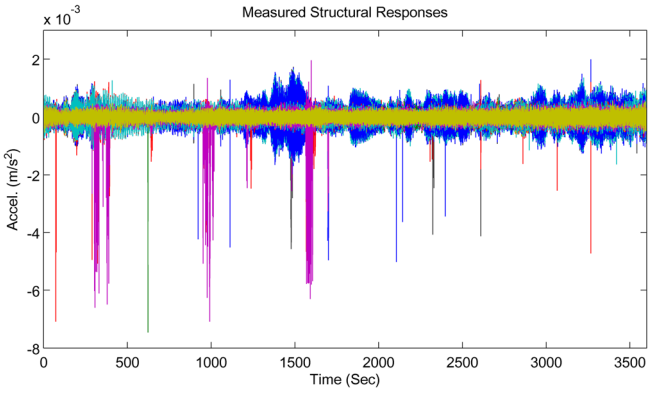

Figure 1. The recorded ambient vibration accelerations of the Canton Tower from 12:00 January 20, 2010 to 13:00 January 20, 2010 (data for 20 channels are shown, available in [16], and will be detailed in Section 7).

DOI: 10.1002/stc

the multivariate data set in the presence of sparse gross errors (outliers), greatly improving the robustness of the well-known PCA and quickly extending itself to surprisingly broad modern technology application fields where overwhelmingly high-dimensional data haunt, such as video surveillance, computer vision, and Web data indexing, to name a few [22,33–35].

As mentioned, the established PCP-based denoising method can handle both dense noise and outliers altogether present in the structural response data, which existing denoising methods are incapable of. Furthermore, the proposed re-stacking strategy not only guarantees low-rank representations for PCP denoising of both types of noise but also significantly improves the applicability of the traditional PCA-denoising method when only dense noise is present. Also, the PCP algorithm can be formulated as a convex programming with various efficient numerical solvers; it is suitable for even large-scale data that are recorded in modern structural monitoring system. Detailed numerical experiments show that the PCP method with the re-stacking strategy is extremely effective under broad conditions. Its ability is also demonstrated in denoising the real-measured Canton Tower SHM data set.

2. PCA/SVD DENOISING

2.1. Principal components and vibration modes

Structural vibration responses $\mathbf{x}(t)$ of an n-DOF linear system governed by the second-order equation of motion

$$\mathbf{M}\ddot{\mathbf{x}}(t) + \mathbf{C}\dot{\mathbf{x}}(t) + \mathbf{K}\mathbf{x}(t) = \mathbf{f}(t) \tag{1}$$

can be expressed by the modal expansion as linear combinations of n modal responses $\mathbf{q}(t) = [q_1(t), \ldots, q_n(t)]^T$,

$$\mathbf{x}(t) = \mathbf{\Phi}\mathbf{q}(t) = \sum_{i=1}^{n} \boldsymbol{\varphi}_i q_i(t) \tag{2}$$

$\mathbf{M}$, $\mathbf{C}$, and $\mathbf{K}$ are constant mass, damping, and stiffness matrices, respectively, and are real-valued and symmetric; $\mathbf{\Phi}$ is the inherent vibration mode matrix, whose ith column $\boldsymbol{\varphi}_i$ (mode shape) is associated with $q_i(t)$.

Make t implicit, and denote the measured structural response matrix $\mathbf{X} \in \mathbb{R}^{m\times N}$ with m sensors and N time history sampling points ($m < N$), its SVD representation is

$$\mathbf{X} = \mathbf{U}\Sigma\mathbf{V}^T = \sum_{i=1}^{r} \sigma_i \mathbf{u}_i \mathbf{v}_i^T \tag{3}$$

where $\mathbf{U} = [\mathbf{u}_1, \ldots, , \mathbf{u}_m] \in \mathbb{R}^{m\times m}$ is an orthonormal matrix associated with the sensor dimension, called left-singular vectors or principal components; $\mathbf{\Sigma} \in \mathbb{R}^{m\times N}$ has m diagonal elements σ_i as the ith singular value ($\sigma_1 > \ldots > \sigma_r > \sigma_{r+1} = \ldots = \sigma_m = 0$), and $\mathbf{V} = [\mathbf{v}_1, \ldots, , \mathrm{v_N}] \in \mathbb{R}^{N\times N}$ is associated with the time history dimension, called the right-singular vector matrix. SVD is closely related to the eigenvalue decomposition (EVD); for example, the left-singular vector matrix $\mathbf{U}$ is obtained by the EVD of its covariance matrix

$$\mathbf{X}\mathbf{X}^T = \mathbf{U}\overline{\Sigma}^2\mathbf{U}^T \tag{4}$$

and similarly for $\mathbf{V}$.

It is well understood that the ith singular value σ_i is related to the energy captured by the ith principal component (direction) of $\mathbf{X}$. In structural dynamics, under some assumption, the principal components would coincide with the mode directions [36] with the corresponding singular values indicating their participating energy in the structural responses $\mathbf{X}$, that is, the structural active modes are captured by r principal components.

DOI: 10.1002/stc

2.2. PCA denoising

If $\mathbf{X}$ is contaminated by small dense noise $\mathbf{N}_0$,

$$\hat{\mathbf{X}}=\mathbf{X}_0+\mathbf{N}_0 \tag{5}$$

then denoising can be achieved by keeping only the r principal components with largest singular values, where the modal components are dominant over the noise, while others dominated by noise are abandoned. Such a strategy is termed PCA denoising; if $\mathbf{N}_0$ is small and independent and identically distributed Gaussian, it is optimal in an ℓ_2 sense and can be realized by the following program:

$$(P_2): \quad \text{minimize} \quad \left\|\hat{\mathbf{X}}-\mathbf{X}\right\|_{\ell_2} \text{ subject to } \operatorname{rank}(\mathbf{X}) \leqslant r \tag{6}$$

where $\|\mathbf{X}\|_{\ell_2}=\sigma_1(\mathbf{X})$. From the aforementioned equations, it can be observed that (traditional) PCA denoising would require $m>r$, that is, the sensor number needs to be larger than that of the involved modes (such a requirement is in fact a common assumption where PCA is found effective such as in damage identification and feature extraction [37–39]), which is not known a priori, however. Empirical thresholding would then be demanded in practice, say, keeping only r' largest principal components. However, even one single outlier in the measurement $\hat{\mathbf{X}}$ would cause (P_2) to completely fail in finding the true $\mathbf{X}_0$, because the ℓ_2-minimization does not account for such grossly corrupted error, which, unfortunately, is ubiquitous in practice. Robust PCA technique, PCP, explicitly handles both small dense noise and large outliers, as detailed in the following text.

3. PCP DENOISING

Robust PCA [22,23], termed PCP, is capable of dealing with the most challenging denoising problem—when the original data $\mathbf{X}\in\mathbb{R}^{m\times N}$ are addictively corrupted by both gross errors (outliers) and dense noise,

$$\hat{\mathbf{X}}=\mathbf{X}_0+\mathbf{N}_0+\mathbf{Z}_0 \tag{7}$$

where $\mathbf{Z}_0\in\mathbb{R}^{m\times N}$ has few (sparse) but gross outlier elements with arbitrarily large and located magnitudes and $\mathbf{N}_0\in\mathbb{R}^{m\times N}$ is entry-wise independent and identically distributed small dense noise. PCP aims to recover $\mathbf{X}_0$ by solving the following convex program:

$$(P_1): \quad \text{minimize} \quad \|\mathbf{X}\|_*+\lambda\|\mathbf{Z}\|_{\ell_1} \text{subject to } \left\|\hat{\mathbf{X}}-\mathbf{X}-\mathbf{Z}\right\|_{\mathrm{F}}\leqslant\delta \tag{8}$$

where $\|\mathbf{X}\|_*:=\sum_i\sigma_i(\mathbf{X})$ is termed the nuclear norm of the matrix $\mathbf{X}$, which summates its singular values; $\|\mathbf{Z}\|_{\ell_1}:=\sum_{ij}|z_{ij}|$ denotes the ℓ_1-norm of the matrix $\mathbf{Z}$, which is thought as a long vector; $\lambda=1/\sqrt{N}$ is a trading parameter, $\|\mathbf{X}\|_{\mathrm{F}}:=\sqrt{\sum_i\sigma_i^2}$ is the Frobenius norm of $\mathbf{X}$, and δ is some bounding parameter related to the small dense noise level.

The nuclear norm is the convex approximation to the rank of a matrix, and the ℓ_1-norm is the tightest convex relaxation to the well-known sparsity measure ℓ_0-norm that simply counts the non-zero entries of a matrix. (P_1) can be interpreted as finding the $\mathbf{X}_0^*$ with smallest rank and $\mathbf{Z}_0^*$ with sparsest representation that explain the observation $\hat{\mathbf{X}}$ within a bounded noise level δ.

Candès *et al*. [22,23] rigorously proves that under surprisingly broad conditions, with overwhelmingly high probability, (P_1) accurately recovers the true low-rank $\mathbf{X}_0$ and sparse $\mathbf{Z}_0$. Note that (P_1) assumes no any a priori knowledge of $\mathbf{X}_0$'s rank or the distribution of the singular values, or the magnitudes and locations of the non-zero entries (outliers) of $\mathbf{Z}_0$; all it requires are that $\mathbf{X}_0$ is indeed low-rank and $\mathbf{Z}_0$ sparse. The detailed proof is found in [22,23].

The convex (P_1) program can be implemented using an augmented Lagrange multiplier (ALM) method [40]. Inheriting from the virtue of convex program, the solution to (P_1) found by ALM is always globally optimal.

DOI: 10.1002/stc

4. GUARANTEED LOW-RANK REPRESENTATION

The PCP technique with (P_1) program is straightforward and tempting for the robust denoising problem. First, the good news is that the outliers or gross errors $\mathbf{Z}_0 \in \mathbb{R}^{m\times N}$ present in the signals are indeed sparse as indicated by their nature. On the other hand comes the bad news that $\mathbf{X}_0 \in \mathbb{R}^{m\times N}$, which is aimed to be recovered from the noisy measurements $\hat{\mathbf{X}} \in \mathbb{R}^{m\times N}$, is seldom (if ever) low rank: for civil engineering structures, typically large-scale, the sensor number m is not so much more than (often times even less than) the involved r modes; as a result, $r \ll m$ cannot be guaranteed for a low-rank representation. In fact, this assumption commonly made in previous literatures can seldom be realized in practice that sensor numbers are larger than involved vibration modes. On the one hand, as mentioned, civil engineering structures are typically large scale and may have numerous active modes; on the other, when subject to complex or varying excitation, the mode number excited out can be time variant.

Fortunately, the weak assumption for the success of PCP serves as the key to constructing a low-rank representation of the structural response matrix for robust denoising. Divide the time history of each channel, say, $\mathbf{x}_i \in \mathbb{R}^N$ (ith channel), into l segments, yielding $(\mathbf{x}_i)_j \in \mathbb{R}^v$ as the jth segment of $\mathbf{x}_i$, where $v = N/l$. Then, re-stack them into a new structural response matrix $\overline{\mathbf{X}} \in \mathbb{R}^{w\times v}$,

$$\overline{\mathbf{X}} = \overline{\mathbf{X}}_0 + \overline{\mathbf{Z}}_0 + \overline{\mathbf{N}}_0 \tag{9}$$

where $w = m \times l, \overline{\mathbf{X}}_0, \overline{\mathbf{Z}}_0, \overline{\mathbf{N}}_0 \in \mathbb{R}^{w\times v}$. Such a strategy can be seen as enhancing each original spatial sensor with l 'virtual' temporal sensors. Because there are still only r modes involved in the re-stacked matrix $\overline{\mathbf{X}} \in \mathbb{R}^{w\times v}$,

$$\operatorname{rank}\left(\overline{\mathbf{X}}\right) \approx r \ll \min(w, v) \tag{10}$$

that is, $\overline{\mathbf{X}}$ becomes a low-rank matrix. In addition, both the ℓ_1-norm and Frobenius norm of a matrix are summations of its entries and energy, respectively; as such, restacking would not essentially change the property that $\overline{\mathbf{Z}}_0 \in \mathbb{R}^{w\times v}$ remains sparse and $\overline{\mathbf{N}}_0 \in \mathbb{R}^{w\times v}$ bounded. With these assumptions satisfied, (P_1) accurately estimates the low-rank $\overline{\mathbf{X}}_0 \in \mathbb{R}^{w\times v}$ (and the outliers $\overline{\mathbf{Z}}_0 \in \mathbb{R}^{w\times v}$), which can then be readily re-stacked back to $\mathbf{X}_0^* \in \mathbb{R}^{m\times N}$.

Note that the re-stacking guaranteeing low-rank representation also benefits the traditional PCA denoising when the outliers are absent, as it removes the constraint that the sensor number $m > r$ (to ensure redundancy). Besides, Equation (10) suggests re-stacking $\overline{\mathbf{X}} \in \mathbb{R}^{w\times v}$ as square as possible, but this needs not to be exactly so in practice, as will be illustrated by various examples in Section 6. It is also interesting to note a somewhat obvious yet strange fact that long time history (large N) is advantageous for a low-rank representation and hence the success of PCP denoising: large-scale data set is in fact more welcome, but the computation burden will of course increase.

5. PCP DENOISING STRATEGY

The proposed PCP denoising scheme is able to simultaneously remove both dense noise and gross outliers under broad conditions for success; its implementation is straightforward and efficient, following these steps:

Step 1. According to the matrix dimension, choose a reshape factor l that would make the new structural response data matrix roughly square.
Step 2. Perform PCP on the shaped structural response matrix to recover the low-rank matrix.
Step 3. Re-stack the recovered low-rank matrix back to the structural response matrix in its original shape as the estimation of the clean structural response data.

6. NUMERICAL SIMULATION

6.1. Model setup

To demonstrate the performance of the proposed PCP denoising algorithm, numerical simulations are conducted on a 12-DOF linear time-invariant mass–spring damped model (Figure 2) in this section.

DOI: 10.1002/stc

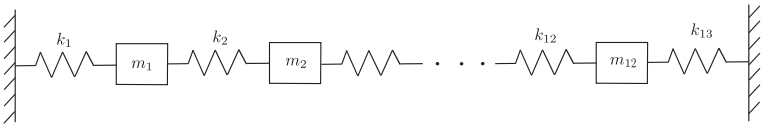

Figure 2. The numerical 12-DOF linear lumped mass–spring damped model.

The parameters are set as follows: the lumped mass is $m_1 = 2$, $m_2 = \ldots = m_{11} = 1$, $m_{12} = 3$, the spring stiffness is $k_1 = \ldots = k_{13} = 1$, and proportional damping is considered with respect to the mass matrix as $\mathbf{C} = \alpha \mathrm{M}$ with different values of α to account for different damping levels (as will be detailed later). Both free vibration and random vibration are studied. Newmark-Beta algorithm is used to obtain time histories of the system responses. The sampling frequency is set at 10 Hz, and the time histories 2000 s, ending up with $N = 20000$ samples at each of the $m = 12$ channels, that is, the structural response matrix $\mathbf{X}_0 \in \mathbb{R}^{12\times 20000}$.

6.2. Performance results

6.2.1. Reshape and low-rank representations. This section first shows that the strategy of re-stacking the structural response matrix makes low-rank representations that are desired for effective de-noising. Free vibration is induced by initial impact at the 12th DOF, and random vibration is generated by applying zero-mean Gaussian white noise (GWN) at the 12th DOF to excite the structure. Different reshape factors l are applied to re-stack the original clean $\mathbf{X}_0 \in \mathbb{R}^{12\times 20000}$; for example, if $l = 40$, then $w = 12 \times 40 = 480$, and $v = 20000/40 = 500$, then the re-stacked $\overline{\mathbf{X}}_0 \in \mathbb{R}^{480\times 500}$, and so on. After conducting SVD on the re-stacked matrix, the singular values are shown from Figure 3 for free and random vibration cases. They indicate that the singular values vanish fast for all the re-stacked matrices, that is, the rank of $\overline{\mathbf{X}}_0$, r, is small. Take $l = 40$ for example again, $r \ll \min(w,v) = 480$, that is, $\overline{\mathbf{X}}_0 \in \mathbb{R}^{480\times 500}$ is indeed a low-rank matrix that may be targeted by the PCP if corrupted by noise in practice, whose performance will be shown in the following section. In contrast, for the original $\mathbf{X}_0 \in \mathbb{R}^{12\times 20000}$ ($l = 1$), although r is small, $\min(w,v) = 12$, which does not make a low-rank matrix.

6.2.2. PCP denoising of outliers and comparison with PCA. With the re-stacking strategy, the performance of PCP can be applied to simultaneously denoise both dense noise and gross outliers. Dense noise modeled as zero-mean GWN (signal-to-noise ratio (SNR) = 20 dB or 10% root mean square noise level with respect to the original clean signal) is first added to the structural response $\mathbf{X}_0 \in \mathbb{R}^{12\times 20000}$ at each channel, and then 1% outliers (i.e., 2400 entries out of the $12 \times 20,000 = 240,000$ ones) are distributed uniformly at random among the matrix with normally distributed magnitudes (zero-mean and 10 variance) multiplied by the standard deviation of the first displacement $\mathbf{x}_1 \in \mathbb{R}^{20000}$; the measured noisy data matrix is therefore $\hat{\mathbf{X}}_0 \in \mathbb{R}^{12\times 20000}$ with both dense noise and sparse outliers. Note that these noise parameters are used as protocol examples here, and the PCP performance under different conditions will be additionally presented in Section 6.2.3; also, the first channel signal is shown for illustrations.

A reshape factor $l = 40$ is used, and the PCP is applied to decompose the re-stacked $\overline{\mathbf{X}} \in \mathbb{R}^{480\times 500}$, and it is shown that the PCP accurately recovers the original clean structural responses from the corrupted measurements in free vibration (Figures 4 and 5) and in random vibration (Figures 6 and 7). Take the free vibration case for example, Figure 4 shows that the noisy measurement with both dense noise and gross outliers is smoothly denoised by PCP, and the PCP-denoised signal matches the original clean signal very well as shown in Figure 5. Besides, Figures 8 and 9 show that the PCP also works well in case the structural damping is high ($\alpha = 0.1$ and the damping ratio is as high as 21.0%) and the sensor number is as limited as $m = 6$. This is expected, because the underlying reshaped structural response matrix (original clean) indeed has a low-rank representation (Figure 3) and the outliers are unknown but sparse such that PCP accurately and stably decomposes them from the noisy measurements.

DOI: 10.1002/stc

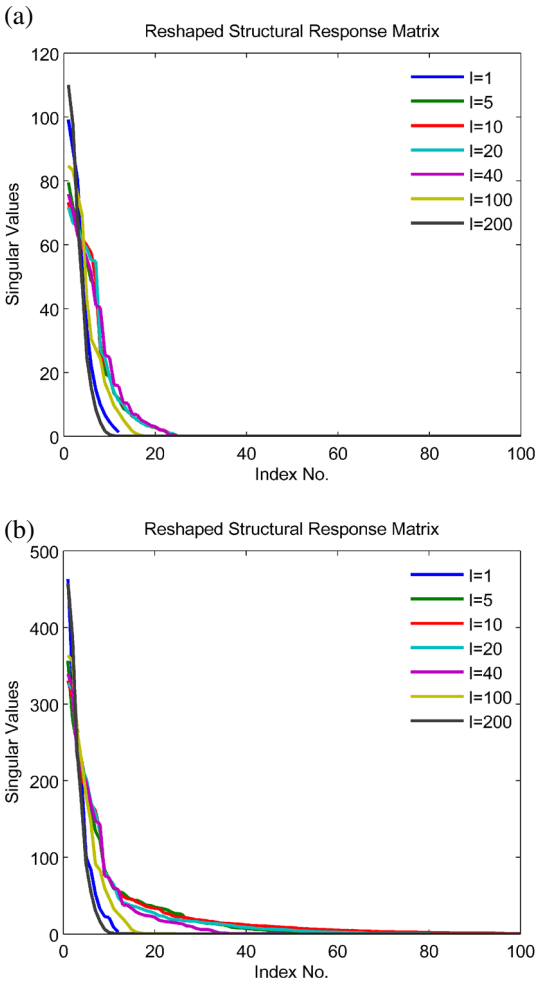

Figure 3. Singular values of the reshaped structural response data matrices of the 12-DOF model with different reshaping factors: (a) in free vibration and (b) in random vibration, $\alpha = 0.001$ (the index of the singular values is shown up to 100).

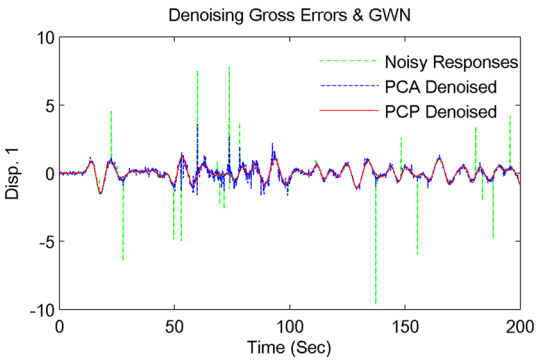

Figure 4. PCP and PCA denoising with re-stacking strategy of the structural responses with both GWN and gross outliers of the 12-DOF model in *free* vibration (channel 1), reshaped factor $l = 40$, $\alpha = 0.001$; 0–200 s is shown for visual enhancement.

The PCA-denoising scheme is also conducted for comparisons. Figure 10(a) shows that in the original dimension, the singular values of the noisy structural response matrix $\hat{\mathbf{X}}_0 \in \mathbb{R}^{12\times 20000}$ do not vanish whether they are corrupted by only GWN or by both gross outlier and GWN. As shown in Figure 10(b),

DOI: 10.1002/stc

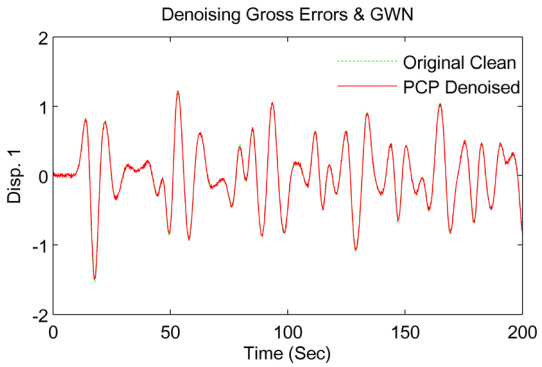

Figure 5. The PCP-denoised structural responses (channel 1) in *free* vibration (reshape factor $l = 40$) of the 12-DOF model compared with the original clean (no noise) signal, $\alpha = 0.001$ (only 0–200 s is shown).

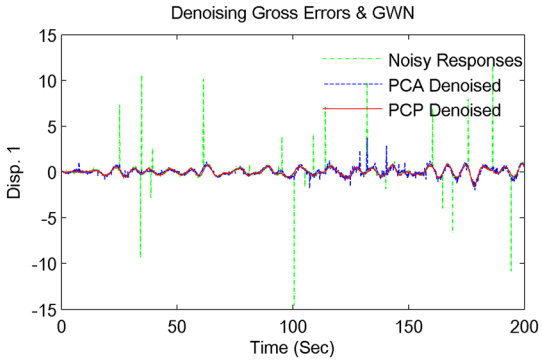

Figure 6. PCP and PCA denoising with re-stacking strategy of the structural responses with both GWN and gross outliers of the 12-DOF model in *random* vibration (channel 1), reshaped factor $l = 40$, $\alpha = 0.001$; 0–200 s is shown for visual enhancement.

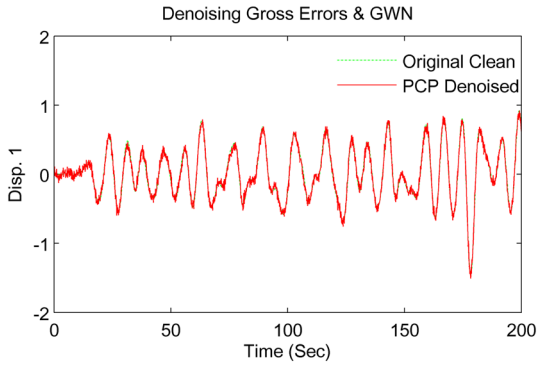

Figure 7. The PCP-denoised structural responses (channel 1) in *random* vibration (reshape factor $l = 40$) of the 12-DOF model compared with the original clean (no noise) signal, $\alpha = 0.001$ (only 0–200 s is shown).

although re-stacking to $\overline{\mathbf{X}} \in \mathbb{R}^{480\times 500}$ makes its singular values decay fast when only GWN is present, outliers immediately destroy it: this explains why PCA-denoising scheme of truncating the less significant principal components fails whenever gross outliers are present, as already shown in Figures 4–9.To quantitatively measure their performance, the recovery error at the ith channel is measured by

$$\in_i = \frac{\left\|\mathbf{x}_i^{'} - \mathbf{x}_i\right\|_{\ell_2}}{\left\|\mathbf{x}_i\right\|_{\ell_2}} \tag{11}$$

DOI: 10.1002/stc

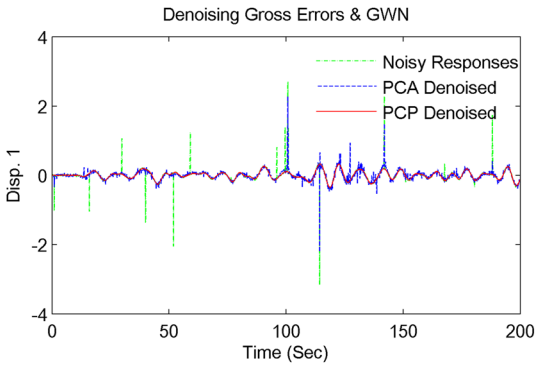

Figure 8. PCP and PCA denoising with re-stacking strategy of the structural responses with both GWN and gross outliers of the 12-DOF model in *random* vibration when only six sensor data are available, reshaped factor $l = 40$, $\alpha = 0.1$; 0–200 s of channel 1 is shown.

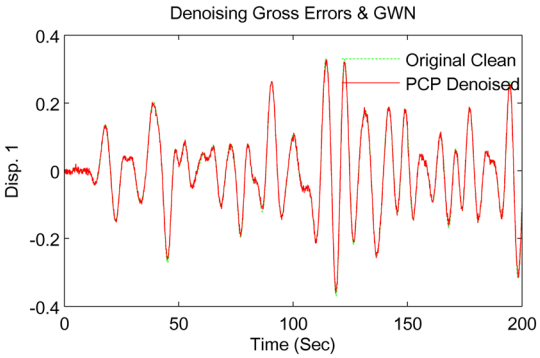

Figure 9. The PCP-denoised structural responses (channel 1) in *random* vibration (reshape factor $l = 40$) of the 12-DOF model when only six sensor data are available, compared with the original clean (no noise) signal (channel 1), $\alpha = 0.1$ (only 0–200 s is shown).

or in an SNR measure

$$\mathrm{SNR} = 20\log_{10}\frac{\mathrm{RMS}(\mathbf{x}_i)}{\mathrm{RMS}(\mathbf{x}_i' - \mathbf{x}_i)} \tag{12}$$

where $\mathbf{x}_i$ and $\mathbf{x}_i'$ are the original clean signal and the de-noised signal at the ith channel. Table I shows that PCP clearly outperforms PCA in simultaneously denoising both outliers and dense noise.

6.2.3. PCP denoising performance under different situations. In Section 4, it is formulated that PCP may work very well under broad conditions; this section studies a wide range of situations to show that it is so.

First, different percentages of gross outliers (1–20%, also randomly distributed) and different magnitudes (the variance is multiplied by 5–100 times) are added, and the dense noise is kept at 20 dB level. Using a reshape factor $l = 40$, the PCP denoising results are depicted with different percentages of outliers in Figure 11(a) and with different magnitudes of outliers in Figure 11(b). Clearly, in all cases, the recovery error (averaged per channel) is very small in the order of 10^{-3}. This means that PCP is not sensitive to the outlier amount and magnitude: PCP can remove even many arbitrarily large gross errors.

Different dense noise levels are also studied from SNR = 5–30 dB (noise as high as 39.81% to 3.16%), and Figure 12 shows that PCP works stably: the recovery error increases reasonably as the noise level increases.

Although Equation (10) suggests that it is best to choose a reshape factor that makes an approximately square matrix to ensure it is 'most low-rank', it may cost more computational effort with more

DOI: 10.1002/stc

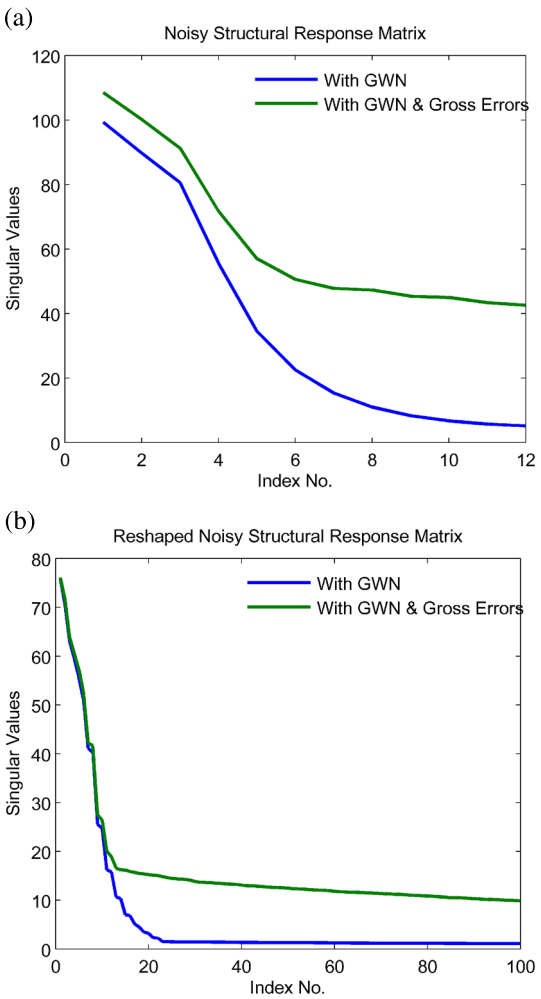

Figure 10. Singular values of the structural response data matrix of the 12-DOF model in free vibration with only GWN or with both GWN and gross outliers, $\alpha = 0.001$, (a) in its original dimension 12×20000 and (b) using a reshape factor $l = 40$ so that it has a shape of 480×500 (the index of the singular values is shown up to 100).

Table I. Denoising performance of PCP and PCA with gross outliers and dense GWN (reshape $l = 40$).

	Free vibration				Random vibration			
	SNR (dB)		Error (%)		SNR (dB)		Error (%)	
Channel	PCP	PCA	PCP	PCA	PCP	PCA	PCP	PCA
1	50.36	12.48	0.30	23.76	48.56	14.24	0.37	19.41
2	50.33	19.52	0.30	10.57	48.74	15.95	0.37	15.94
3	50.09	18.45	0.31	11.95	49.20	17.30	0.35	13.65
4	50.23	16.68	0.31	14.66	49.39	19.93	0.34	10.09
5	49.92	20.64	0.32	9.29	48.93	19.85	0.36	10.18
6	49.89	15.05	0.32	17.69	48.73	13.95	0.37	20.07
7	50.20	19.07	0.31	11.13	48.21	15.50	0.39	16.80
8	50.14	8.76	0.31	36.50	48.73	16.95	0.37	14.20
9	50.12	18.99	0.31	11.23	49.03	22.21	0.35	7.75
10	49.91	18.95	0.32	11.28	48.87	18.61	0.36	11.73
11	49.84	13.47	0.32	21.21	48.37	15.01	0.38	17.77
12	51.50	22.35	0.27	7.63	48.65	19.07	0.37	11.13

DOI: 10.1002/stc

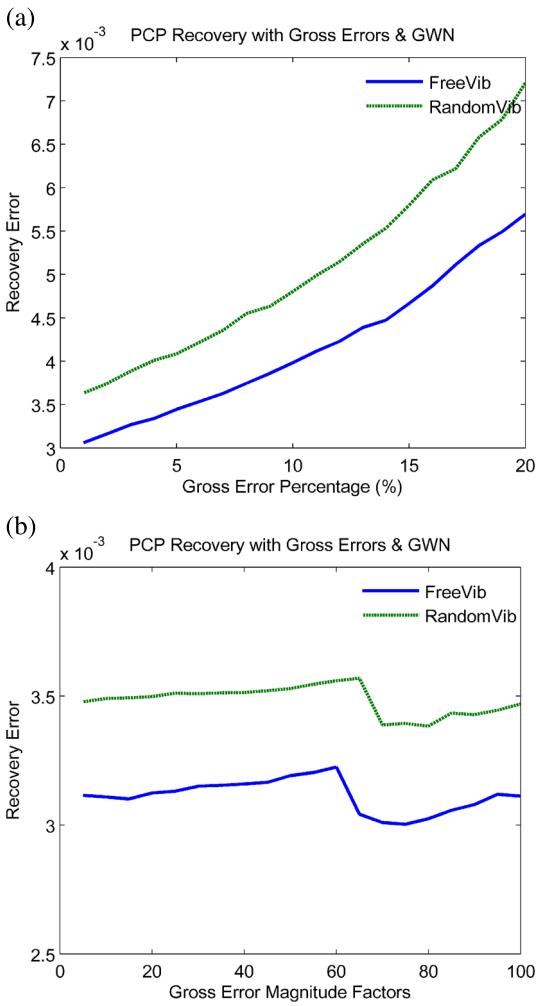

Figure 11. The recovery errors (averaged per channel) of the PCP denoising of the structural responses (reshape factor $l = 40$) of the 12-DOF model, $\alpha = 0.001$: (a) with different percentages of gross outliers and (b) with different magnitudes of the gross outliers.

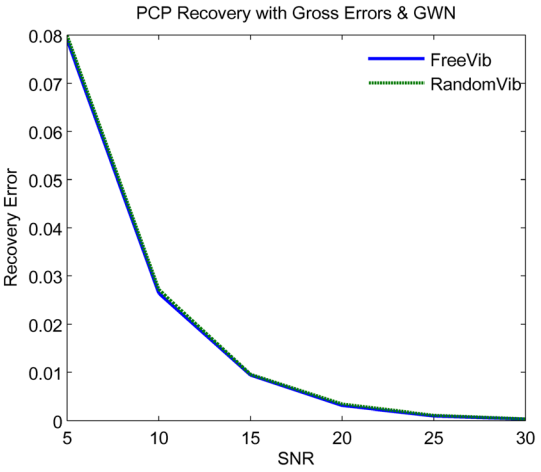

Figure 12. The recovery errors (averaged per channel) of the PCP denoising of the structural responses of the 12-DOF model with different SNR levels, $\alpha = 0.001$, $l = 40$.

DOI: 10.1002/stc

'virtual sensors'. To see whether there is a balance, different reshape factors are used and PCP is performed, and the computation time is recorded. Figure 13(a) indicates that the recovery error immediately experiences a significant drop even for a slight reshape factor $l=5$, and around $l=40$, the recovery error has been very small. Referring to the computation time shown in Figure 13(b), it grows roughly linearly with the reshape factor. The balance tends to be around $l=40$, which makes the re-stacked matrix most close to square matrix, although as shown in Figure 13(a), it does not necessarily need to be so in practice, as a wide range of choices of reshape factors have achieved very good denoising effects with very small recovery errors.

7. APPLICATION ON CANTON TOWER SHM DATA

The proposed PCP denoising scheme is applied on the real-measured SHM data of the Canton Tower in this section (Figure 14). The Canton Tower is a high-rise tall building of 610 m, located in Guangzhou City, China; more description of this structure is found in [12]. An advanced SHM system has been instrumented with more than 800 various types of sensors to continuously monitor its performance during construction and service stages. In particular, an SHM benchmark problem was established on the basis of full-scale field measurements; a set of 24-h ambient vibration data recorded from 18:00 January 19, 2010 to 18:00 January 20, 2010 is provided on the website [16]. Twenty

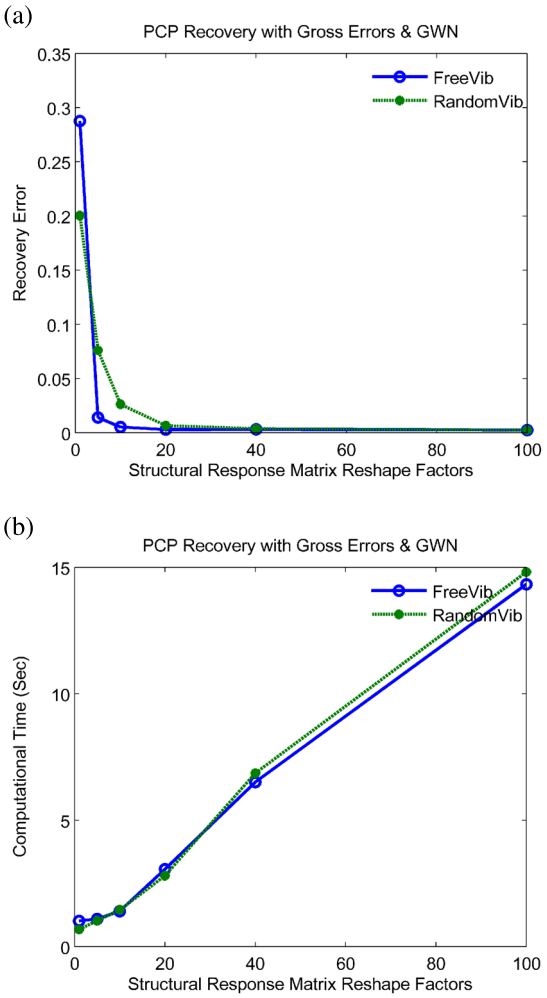

Figure 13. (a) The recovery error and (b) the computational time of the PCP denoising of the structural responses of the 12-DOF model using different reshape factors from $l=1$ to $l=100$, $\alpha=0.001$.

DOI: 10.1002/stc

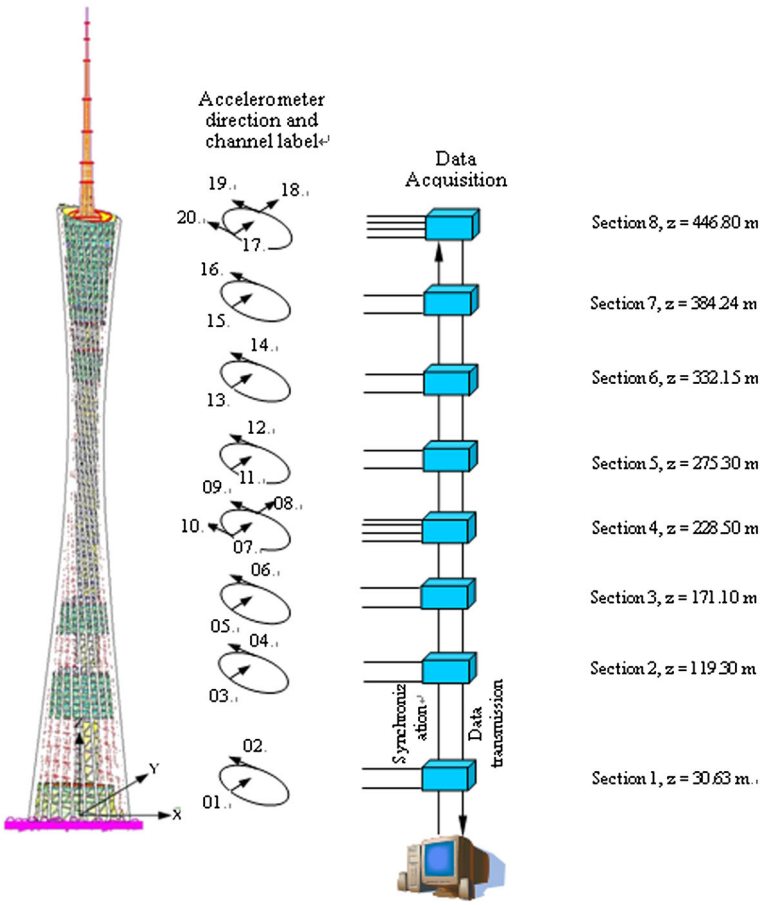

Figure 14. The sensor outline of the ambient vibration testing of the Canton Tower. The number and arrow denote the sensor number and measurement axis, respectively.

uni-axial accelerometers, whose layout is shown in Figure 8, were used to record the structural responses in the *X* and *Y* axes, with a sampling frequency of 50 Hz. A few researchers have conducted the system identification of this structure on the basis of this set of data [41–46], but this study only focuses on the denoising problem of the monitoring data.

As shown in Figure 1, remarkable outliers are present in the measured SHM data, which would significantly affect the value of the data for further analysis and identification. The 1-h data from 12:00 January 20 to 13:00 Jan 20, 2010 is used to show the ability of PCP denoising in this study. The measured structural response data matrix is then $\hat{\mathbf{X}} \in \mathbb{R}^{20\times 180000}$. The re-stack scheme is applied with $l = 100$ such that the reshaped $\overline{\mathbf{X}} \in \mathbb{R}^{1800\times 2000}$. The SVD analysis of $\hat{\mathrm{X}}$ shows that the singular values do not vanish whatsoever (Figure 15(a)) and same situation happens for $\overline{\mathbf{X}} \in \mathbb{R}^{1800\times 2000}$: the PCA-denoising scheme would not work, which is mostly caused by the significant outliers.

PCP is used to denoise $\overline{\mathbf{X}}$ and then re-stack back to $\widetilde{\mathbf{X}} \in \mathbb{R}^{20\times 180000}$ (plotted in Figure 16). Clearly, all the outliers are removed by PCP. Looking closely at Figures 17 and 18, it is seen that the outliers are picked out and the denoised signals are smooth (such as in channel 10). Also, as observed in the SVD results (Figure 15(b)), the singular values of the restacked denoised structural responses decay much faster than the noisy re-stacked one, which means that much less noise are present in the denoised signals.

For comparisons, the traditional low-pass filter denoising method with a bandwidth up to 2 Hz is applied to the measured $\hat{\mathbf{X}} \in \mathbb{R}^{20\times 180000}$. Results show that the noise is not effectively removed: Figure 17 shows that the outlier is not removed, and there is obvious phase aliasing in the denoised signal (Figure 18), which does not happen in the PCP-denoised signal.

DOI: 10.1002/stc

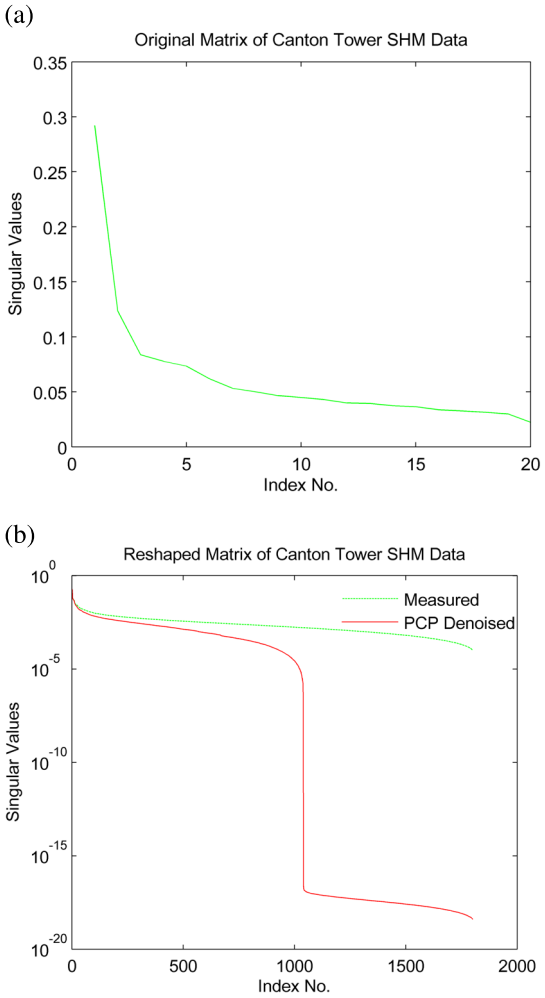

Figure 15. Singular values of the Canton Tower 1-h ambient vibration acceleration matrices: (a) in its original dimension 20×180000 and (b) in reshaped dimension 2000×1800 of the measured data and PCP-denoised data (reshape factor $l = 100$).

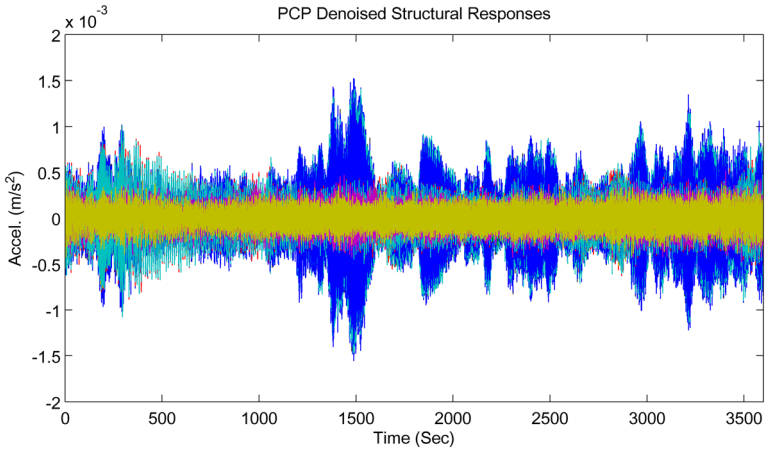

Figure 16. The PCP-denoised (reshape factor $l = 40$) 1-h structural vibration accelerations of the Canton Tower (data for the 20 channels are shown in different colors) (compared with the measured data shown in Figure 1).

DOI: 10.1002/stc

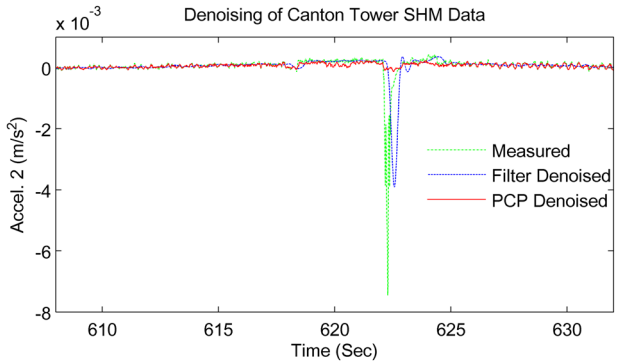

Figure 17. The PCP-denoised and filter-denoised acceleration of channel 2 of the Canton Tower 1-h SHM data compared with the measured data (shown between 605 and 635 s for visual enhancement).

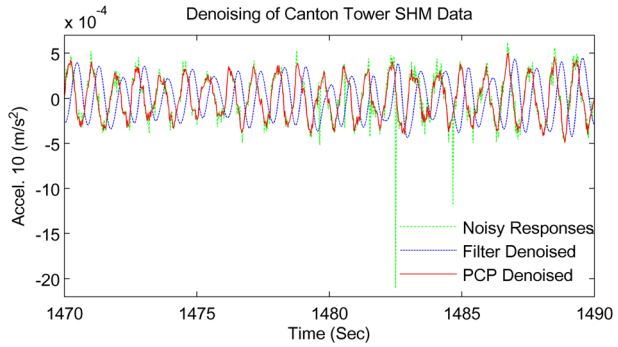

Figure 18. The PCP-denoised and filter-denoised acceleration in channel 10 of the Canton Tower 1-h SHM data compared with the measured data (shown between 1470 and 1490 s for visual enhancement).

8. CONCLUSIONS

This study presents a new denoising scheme for removal of both dense noise and outliers common in the measured structural vibration responses via PCP. A simple and effective strategy of re-stacking the structural vibration responses, which does not essentially change the contained structural dynamic information, is proposed to guarantee a low-rank representation such that the challenging denoising problem can be cast into the powerful PCP framework.

Detailed numerical simulations are conducted, and results show that PCP works well under various conditions in handling both types of noise altogether; especially, the assumption used to be made in traditional PCA method that sensor number is larger than mode number is avoided thanks to the re-stacking strategy, which also improves the traditional PCA-denoising method when only dense noise is present. Also, compared with PCA with thresholding scheme, the PCP denoising scheme needs no any prior information with respect to the distribution and magnitudes of the data matrix's singular values: it can be implemented 'blindly'. The ability of PCP for practical applications is also illustrated in denoising the real-measured monitoring data of the Canton Tower.

The wide success of PCP with the re-stacking strategy in denoising the structural vibration responses would be highly expected for large-scale data analysis in structural dynamics and SHM applications, because it is straightforward, efficient, and reliable.

ACKNOWLEDGEMENTS

The authors are grateful to Prof. Y. Ni and his coworkers at the Hong Kong Polytechnic University for sharing the Canton Tower SHM data on their website [16].

DOI: 10.1002/stc

REFERENCES

1. Cebeli M, Sanli A, Sinclair M, Gallant S, Radulescu D. Real-time seismic monitoring needs of a building owner and the solution: a cooperative effort. *Earthquake Spectra* 2004; **20**:333–346.
2. Celebi M. Recorded earthquake responses from the integrated seismic monitoring network of the Atwood building. *Anchorage, Alaska, Earthquake Spectra* 2006; **22**:847–864.
3. Kohler P, Davis E, Safak E. Earthquake and ambient vibration monitoring of the steel-frame UCLA Factor Building. *Earthquake Spectra* 2005; **21**:715–736.
4. Huang M, Shakal A. Strong motion instrumentation of seismically-strengthened port structures in California by CSMIP, *TCLEE*, 2009.
5. Available from: http://www.conservation.ca.gov/cgs/smip/Pages/Station.aspx.
6. Smyth A, Pei J, Masri S. System identification of the Vincent Thomas suspension bridge using earthquake records. *Earthquake Engineering and Structural Dynamics* 2003; **32**:339–367.
7. Nayeri R, Masri S, Ghanem R, Nigbor R. A novel approach for the structural identification and monitoring of a full-scale 17-story building based on ambient vibration measurement. *Smart Materials and Structures* 2008; **17**:025006.
8. Hong A, Betti R, Lin C. Identification of dynamic models of a building structure using multiple earthquake records. *Structural Control and Health Monitoring* 2009; **16**:178–199.
9. Moaveni B, He X, Conte J, Restrepo J, Panagiotou M. System identification study of a seven-story full-scale building slice tested on the UCSD-NEES shake table. *ASCE Journal of Structural Engineering* 2011; **137**:705–717.
10. Yang Y, Nagarajaiah S. Time-frequency blind source separation using independent component analysis for output-only modal identification of highly-damped structures, *ASCE Journal of Structural Engineering* 2013; **139**(10):1780–1793.
11. Yang Y. Nagarajaiah S. Blind modal identification of output-only structures in time domain based on complexity pursuit, *Earthquake Engineering and Structural Dynamics* 2013; **42**(13):1885–1905.
12. Ni Y, Xia Y, Liao W, Ko J. Technology innovation in developing the structural health monitoring system for Guangzhou New TV Tower. *Structural Control and Health Monitoring* 2009; **16**:73–98.
13. Ni Y, Wong K, Xia Y. Health checks through landmark bridges to sky-high structures. *Advances in Structural Engineering* 2011; **14**:103–119.
14. Li S, Li H, Liu Y, Lan C, Zhou W, Ou J. SMC structural health monitoring benchmark problem using monitored data from an actual cable-stayed bridges. *Structural Control and Health Monitoring* 2013. DOI:10.1002/stc.1559.
15. Farrar C, Worden K. An introduction to structural health monitoring. *Philosophical Transactions of the Royal Society A* 2007; **365**:303–315.
16. Available from: http://www.cse.polyu.edu.hk/benchmark/.
17. Yang W, Tse P. Development of an advanced noise reduction method for vibration analysis based on singular value decomposition. *NDT&E International* 2003; **36**:419–432.
18. Jiang X, Mahadevan S, Adeli H. Bayesian wavelet packet denoising for structural system identification. *Structural Control and Health Monitoring* 2007; **14**:333–356.
19. Hou S, Liang M, Li Y. An optimal global projection denoising algorithm and its application to shaft orbit purification. *International Journal of Structural Health Monitoring* 2011; **10**:603–616.
20. Zhou C, Zhang Y. Particle filter based noise removal method for acoustic emission signals. *Mechanical Systems and Signal Processing* 2012; **28**:63–77.
21. Baneen U, Kinkaid NM, Guivant JE, Herszberg I. Vibration based damage detection of a beam-type structure using noise suppression method. *Journal of Sound and Vibration* 2012; **331**:1777–1788.
22. Candès E, Li X, Ma Y, Wright J. Robust principal component analysis. *Journal of ACM* 2009; **58**:1–37.
23. Zhou Z, Li X, Wright J, Candès E, Ma Y. Stable principal component pursuit, preprint, 2010.
24. Bruckstein A, Donoho D, Elad M. From sparse solutions of systems of equations to sparse modeling of signals and images. *SIAM Review* 2008; **51**:34–81.
25. Baraniuk R, Candès E, Elad M, Ma Y. Application of sparse representation and compressive sensing. *Proceedings of the IEEE* 2010; **98**:906–909.
26. Candès E, Romberg J, Tao T. Robust uncertainty principles: exact signal reconstruction from highly incomplete frequency domain. *IEEE Transactions on Information Theory* 2006; **52**:489–509.
27. Donoho DL. Compressed sensing. *IEEE Transactions on Information Theory* 2006; **52**:1289–1306.
28. Baraniuk RG. *Compressive sensing. IEEE Signal Processing Magazine* 2007; **24**:118–121.
29. Bao Y, Beck JL, Li H. Compressive sampling for accelerometer signals in structural health monitoring. *International Journal of Structural Health Monitoring* 2011; **10**:235–246.
30. Mascarenas D, Cattaneo A, Theiler J, Farrar C. Compressed sensing techniques for detecting damage in structures. *International Journal of Structural Health Monitoring* 2013; in press. DOI: 10.1177/1475921713486184.
31. O'Connor SM, Lynch JP, Gilbert AC. Implementation of a compressive sampling scheme for wireless sensors to achieve energy efficiency in a structural health monitoring system. SPIE Smart Structures and Materials + Nondestructive Evaluation and Health Monitoring, San Diego, CA, 2013.
32. Yang Y, Nagarajaiah S. Output-only modal identification with limited sensors using sparse component analysis. *Journal of Sound and Vibration* 2013; **332**:4741–4765.
33. Min K, Zhang Z, Wright J, Ma Y. Decomposition background topics from keywords by principal component pursuit. In *Proceedings of the 19th ACM International Conference on Information and Knowledge Management*. ACM: New York, NY, USA, 2010; 269–278.
34. Ji H, Liu C, Shen Z, Xu Y. Robust video denoising using low rank matrix completion. In *Proceedings of the 23rd IEEE Conference on Computer Vision and Pattern Recognition*. San Francisco, CA, 2010; 1791–1798.
35. Peng Y, Ganesh A, Wright J, Xu W, Ma Y. RASL: robust alignment by sparse and low-rank decomposition for linearly correlated images. *IEEE Transactions on Pattern Analysis and Machine Intelligence* 2012; **34**:2233–2246.
36. Feeny B, Kappagantu R. On the physical interpretation of proper orthogonal modes in vibration. *Journal of Sound and Vibration* 1998; **211**:607–616.
37. De Boe P, Golinval J-C. Principal component analysis of a piezo-sensor array for damage localization. *International Journal of Structural Health Monitoring* 2003; **2**:137–144.

38. Friswell MI, Inman DJ. Sensor validation for smart structures. *Journal of Intelligent Material Systems and Structures* 1999; **10**:973–982.
39. Kerschen G, De Boe P, Golinval J, Worden K. Sensor validation using principal component analysis. *Smart Materials and Structures* 2005; **14**:36–42.
40. Lin Z, Chen M, Wu L, Ma Y. The augmented Lagrange multiplier method for exact recovery of corrupted low-rank matrices, *UIUC Technical Report UILU-ENG-09-2215,* 2009.
41. Faravelli L, Ubertini F, Fuggini C. Subspace identification of the Guangzhou New TV Tower. In *Proceedings of the 5th World Conference on Structural Control and Monitoring*. Tokyo, Japan, 2010.
42. Chen W, Lu Z, Lin W, Chen S, Ni Y, Xia Y, Liao W. Theoretical and experimental modal analysis of the Guangzhou New TV Tower. *Engineering Structures* 2011; **33**:3628–3646.
43. Ye X, Yan Q, Wang W, Yu X, Zhu T. Output-only modal identification of Guangzhou New TV Tower subject to different environmental effects. In *Proceedings of the 6th Workshop on Advanced Smart Materials and Smart Structures Technology*. Paper No. 076 Dalian, China, 2011.
44. Niu Y, Kraemer P, Fritzen C. Operational modal analysis for the Guangzhou New TV Tower. In *Proceedings of the 29th International Modal Analyis Conference*. Jacksonville, FL, USA, 2011; 211–220.
45. Liu Y, Loh C, Ni Y. Stochastic subspace identification for output-only modal analysis: application to super high-rise tower under abnormal loading condition. *Earthquake Engineering and Structural Dynamics* 2012. DOI:10.1002/eqe.2223.
46. Kuok S, Yuen K. Structural health monitoring of Canton Tower using Bayesian framework. *Smart Structures and Systems* 2012; **10**:375–391.

DOI: 10.1002/stc